

Cotranslational Protein Folding within the Ribosome Tunnel Influences Trigger-Factor Recruitment

Ku-Feng Lin,[†] Chia-Sui Sun,^{†‡} Yi-Chen Huang,^{†¶} Sunney I. Chan,[†] Jiri Koubek,^{§||} Tzong-Huah Wu,[†] and Joseph J.-T. Huang^{†*}

[†]Institute of Chemistry, [‡]Molecular Medicine Program, Taiwan International Graduate Program, Institute of Biomedical Sciences, and [§]Chemical Biology and Molecular Biophysics Program, Taiwan International Graduate Program, Institute of Chemistry, Academia Sinica, Nankang, Taipei, Taiwan; [¶]Graduate Institute of Life Sciences, National Defense Medical Center, Neihu, Taipei, Taiwan; and ^{||}Department of Chemistry, National Taiwan University, Taipei, Taiwan

ABSTRACT In recent years, various folding zones within the ribosome tunnel have been identified and explored through x-ray, cryo-electron microscopy (cryo-EM), and molecular biology studies. Here, we generated ribosome-bound nascent polypeptide complexes (RNCs) with different polyalanine (poly-A) inserts or signal peptides from membrane/secretory proteins to explore the influence of nascent chain compaction in the *Escherichia coli* ribosome tunnel on chaperone recruitment. By employing time-resolved fluorescence resonance energy transfer and immunoblotting, we were able to show that the poly-A inserts embedded in the passage tunnel can form a compacted structure (presumably helix) and reduce the recruitment of Trigger Factor (TF) when the helical motif is located in the region near the tunnel exit. Similar experiments on nascent chains containing signal sequences that may form compacted structural motifs within the ribosome tunnel and lure the signal recognition particle (SRP) to the ribosome, provided additional evidence that short, compacted nascent chains interfere with TF binding. These findings shed light on the possible controlling mechanism of nascent chains within the tunnel that leads to chaperone recruitment, as well as the function of L23, the ribosomal protein that serves as docking sites for both TF and SRP, in cotranslational protein targeting.

INTRODUCTION

There is mounting evidence that the ribosome tunnel plays an active role in regulating translation, initial protein folding, and the early translocation process (1). During protein translation, the nascent chain is synthesized at the peptidyl transferase center (PTC), with the elongating polypeptide penetrating residue by residue through an 80–100 Å long and 10–20 Å wide passage within the ribosome large subunit (2–4). This highly irregular tunnel is predominantly composed of ribosomal RNA (~80%) and three ribosomal proteins (designated L4, L22, and L23 in bacteria) (5,6). In the past decade, much attention has been directed toward studying the influence of the ribosomal tunnel on the protein translation process. For instance, the narrowest part of the tunnel (~25 Å away from the PTC), constructed by a β -hairpin loop of L22 and its proximity neighbor, L4, was suggested to induce translation arrest with the SecM nascent polypeptide (7–10). In addition, depletion of the eukaryotic ribosomal protein L39 from the *Saccharomyces cerevisiae* ribosome resulted in a severalfold decrease in translational accuracy (11).

Recent structural and biophysical studies have shown that short polypeptides may adopt compact conformations within the tunnel (12–14), whereas three-dimensional folding appears to be precluded except toward the distal end (15). By monitoring the fraction of pegylated cysteine on the nascent chain with different consecutive polyalanine (poly-A), inves-

tigators were able to confirm and scrutinize the compaction of poly-A at different regions in the ribosome tunnel (13). In addition, cryo-electron microscopy (cryo-EM) reconstruction of the poly-A-containing nascent chains is consistent with the notion that poly-A fragments can adopt helical conformations within the tunnel (14). At this juncture, it is uncertain whether these ribosome-induced conformations can serve as signals for protein targeting. Nevertheless, the compacted conformations of the nascent polypeptide within the tunnel could still be exploited to direct ribosome-mediated processes such as control of the protein translation arrest, adjustment of the open/closed form of the translocon in the endoplasmic reticulum membrane, and recognition of substrate by the signal recognition particle (SRP) (6–9,12,16).

It is generally recognized that the recruitment of chaperones plays a key role in directing protein targeting, assisting protein folding, and preventing protein aggregation. However, the influence of the folding zone within the ribosome tunnel on the chaperone recruitment has remained largely unexplored. In *Escherichia coli*, trigger factor (TF) is the first chaperone that interacts with the nascent polypeptide emerging from the ribosome to prevent aggregation, and serves as a cradle to promote protein folding (17). It has been shown that the chain length and sequence of the nascent chain outside the ribosome influence the binding of TF to ribosome-bound nascent polypeptide complexes (RNCs) (18–20). Further kinetic studies of the binding/release of TF to/from RNCs also indicate that the hydrophobicity of the nascent chains dominates the TF recognition (20).

Submitted August 17, 2011, and accepted for publication April 24, 2012.

*Correspondence: jthuang@chem.sinica.edu.tw

Editor: Patricia Clark.

© 2012 by the Biophysical Society
0006-3495/12/06/2818/10 \$2.00

doi: 10.1016/j.bpj.2012.04.048

However, it is not clear whether interactions of the nascent polypeptide inside the ribosome tunnel during the early stages of cotranslational protein folding also influence the recruitment of TF. To address this issue and to elucidate the nature of these interactions, we introduced helical structural motifs into the nascent polypeptide chain at various folding zones within the *E. coli* ribosome tunnel and examined the effects of compaction on chaperone recruitment. RNCs with poly-A inserts at different locations and fluorophore-attached amino acids were designed and generated. Fluorescent donor and acceptor introduced into these RNCs by fluorescent tRNAs were exploited for the conformational analysis of the nascent chain by time-resolved fluorescence resonance energy transfer (TR-FRET) experiments. We also generated RNCs bearing two different signal sequences and evaluated their effects on TF binding to further corroborate the influence of nascent chain compaction on TF recruitment.

MATERIALS AND METHODS

Materials

We constructed polyalanine and N-terminal signal sequences on pIVEX2.3d-GFP plasmid (Roche, Mannheim, Germany) by applying site-directed mutagenesis and overlap extension polymerase chain reaction (PCR) (21). The cell-free system (T7 High-Yield Protein Expression System) and BODIPY_{FL}-Lys-tRNA^{Lys} were both purchased from Promega (Madison, WI). The gene encoding *E. coli* TF was constructed into a pET21a plasmid (Merck KGaA, Darmstadt, Germany) and then expressed/purified based on a previous protocol (22). The detailed procedures are described in the Supporting Material. The sequences of the primers used here, as well as the anti-oligonucleotides used to generate the different RNCs, are listed in Table S1.

Synthesis of BODIPY₅₇₆-Met-tRNA^{Met}

BODIPY₅₇₆-Met-tRNA^{Met} was prepared as described previously (23). Briefly, tRNA^{Met} (Sigma-Aldrich, St. Louis, MO) was aminoacylated with *E. coli* aminoacyl tRNA-synthetases (Sigma-Aldrich) in the buffer A (20 mM imidazole-HCl (pH 7.5), 150 mM NaCl, 10 mM MgCl₂, 2 mM ATP, 50 μM methionine) and 0.01 U/μl of pyrophosphatase. After incubation at 37°C for 45 min, the reaction was stopped by adding 0.1 × volume of 3 M NaOAc (pH 5.5) followed by phenol extraction and ethanol precipitation. The precipitated Met-tRNA^{Met} was dissolved in the storage buffer (5 mM NaOAc and 2 mM MgCl₂) and kept at -20°C.

Labeling of the Met-tRNA^{Met} with BODIPY 576/589-SE (Invitrogen, Eugene, OR) was carried out in 50 mM NaHCO₃ solution and 20% DMSO at 4°C for 1 h. The fluorophore-labeled tRNA was purified by means of a Nuc-Away kit (Ambion, Austin, TX), concentrated by ethanol precipitation, and stored in the storage buffer at -20°C. The generation of BODIPY₅₇₆-Met-tRNA^{Met} was confirmed by 10% NaOAc-urea-PAGE (24), which was detected by fluorescence imaging using 532 nm laser excitation with a 580 nm bandpass filter on the gel imager (Typhoon; GE Healthcare, Piscataway, NJ) (Fig. S1).

Generation of fluorophore-labeled RNCs with fluorescent tRNAs

The cell-free system (S30 T7 High-Yield Protein Expression System) was used for nascent-polypeptide biosynthesis. In the reaction, we incorporated

the fluorescent donor and acceptor into the nascent chain cotranslationally by using two fluorophore-attached tRNAs (BODIPY_{FL}-Lys-tRNA^{Lys} (Promega) and BODIPY₅₇₆-Met-tRNA^{Met}, respectively). We controlled the lengths of the nascent chains by applying anti-sGFP₃₄ oligonucleotide and RNase H according to the oligodeoxynucleotide-directed mRNA cleavage method (25). In addition, anti-ssrA oligonucleotide was also included to inhibit *trans*-translation of ssrA (26). The reaction was carried out at 37°C for 30 min, followed by RNC purification at 4°C. After a brief centrifugation (13,000 rpm, 10 min), the RNCs in the supernatant of the cell-free product were further purified by ultracentrifugation as described previously (25), except that a TLA120.1 rotor with a maximum relative centrifuging force of 201,000 × *g* was used. The ribosomal pellet was re-suspended in buffer B (10 mM Tris-HCl (pH 7.0), 60 mM NH₄Cl, 10 mM Mg(OAc)₂, 0.5 mM EDTA, and 1 mM DTT) and kept at -80°C. The nascent chains were confirmed to be bound to the ribosome by means of a puromycin replacement assay (25) (see Fig. 2).

The fluorophore-labeled nascent chains were detected in 12% Tris-acetate SDS-PAGE followed by fluorescence imaging using 488 nm laser excitation accompanied by a 520 nm bandpass filter for donor visualization and 532 nm laser excitation with a 580 nm bandpass filter for acceptor visualization (Typhoon; GE Healthcare).

Frequency-domain fluorescence lifetime measurements

Lifetime measurements on the donor fluorophore were performed at room temperature on a multifrequency phase and modulation fluorimeter (Chronos; ISS, Champaign, IL) equipped with a diode laser ($\lambda_{ex}=473$ nm). All samples were detected at 10–200 MHz of modulation frequency with a fluorescent standard, fluorescein (lifetime ~4 ns). An FF01-536/40-25 filter (Semrock) that allowed fluorescence signals from the donor but suppressed noise from the acceptor emission was used in the detection. For each sample, the determination of phase shift and modulation ratio under different modulation frequencies was repeated three times. The averaged information was then applied for the fitting. The total number of measurements from independent experiments (*n*) was 3–6. We analyzed the fluorescence data by using the Vinci software package (ISS) based on the relationships among the phase shift (ϕ), the modulation ratio (*M*), and the fluorescence lifetimes (τ). Details are provided below.

Fitting of the frequency-domain fluorescence lifetimes

We determined the fluorescence lifetimes of the samples using the relative phase shift and the modulation ratio of the fluorescence with respect to the fluorescent reference fluorescein. The relationships among the phase shift (ϕ), modulation ratio (*M*), and lifetimes (τ) are given as follows:

$$\tan \phi = \frac{N_{\omega}}{D_{\omega}}, \quad (1)$$

$$M = (N_{\omega}^2 + D_{\omega}^2)^{1/2}, \quad (2)$$

where

$$N_{\omega} = \frac{\sum_{i=1}^n [\alpha_i \omega \tau_i^2 / (1 + \omega^2 \tau_i^2)]}{\sum_{i=1}^n \alpha_i \tau_i} \quad (3)$$

$$D_\omega = \frac{\sum_{i=1}^n [\alpha_i \tau_i / (1 + \omega^2 \tau_i^2)]}{\sum_{i=1}^n \alpha_i \tau_i}, \quad (4)$$

where n is the number of exponential decays, ω is the angular modulation frequency (radians/s), and τ_i and α_i are the lifetime and the preexponential factor, respectively, of the i th component.

In our experiments, not all of the nascent polypeptides were labeled with fluorescent probes, because the pools of Met-tRNA^{Met} and Lys-tRNA^{Lys} in the protein-expression system were not totally fluorescent-labeled. Although the BODIPY₅₇₆-Met-tRNA^{Met} synthesized for this study had been purified to homogeneity, the fluorescent Met-tRNA^{Met} was subsequently diluted by background endogenous aminoacylated-tRNAs in the cell-free reaction. The incorporation of the BODIPY_{FL}-Lys-tRNA^{Lys} into the nascent chains was expected to be even lower because the BODIPY_{FL}-Lys-tRNA^{Lys} was obtained from a commercial source and was no more than ~80% labeled. Accordingly, some nascent peptides were labeled with the fluorophore at either the donor site or the acceptor site only, and only a small fraction of the nascent polypeptides contained the two fluorophores at the donor and acceptor sites, respectively. In fact, some nascent chains were not fluorescent-labeled at all.

Only those nascent polypeptides containing the Lys labeled with the BODIPY_{FL} would contribute to the emission from the Lys site upon excitation of the fluorophore (donor), and only those chains with both the donor and acceptor sites fluorescent-labeled could give a TR-FRET. Thus, we wrote for the impulse function $I(t)$ as follows:

$$I(t) = \alpha_1 \exp\left(\frac{-t}{\tau_1}\right) + \alpha_2 \exp\left(\frac{-t}{\tau_2}\right) + \alpha_3 \exp\left(\frac{-t}{\tau_3}\right). \quad (5)$$

In this expression, τ_1 comes from light scattering, τ_2 is the lifetime of the donor from nascent chains without the Met fluorescent-labeled, and τ_3 is the shortened lifetime of the donor when there is FRET from the donor to the acceptor fluorophore. Nascent polypeptides that adopt conformations such that the donor and acceptor fluorophores are too far apart to yield measurable FRET will contribute to the τ_2 component. For each component, the corresponding fractional contribution is given by

$$f_i = \left(\frac{\alpha_i \tau_i}{\alpha_1 \tau_1 + \alpha_2 \tau_2 + \alpha_3 \tau_3} \right). \quad (6)$$

When the RNCs are prepared only in the presence of BODIPY_{FL}-Lys-tRNA^{Lys} (donor), the two-exponential model that was used to fit the data as the third component in Eq. 5 no longer carries any physical meaning. The τ_2 obtained from the two-component fit to the data for the donor-labeled RNCs corresponds to the fluorescence lifetime of the donor τ_F^D .

The emission lifetime of the donor is shortened when there is FRET from the donor to the acceptor fluorophore in a nascent chain that is doubly labeled. This lifetime, τ_3 (usually referred to as τ_F^{D+A}), is determined by fitting the results for the donor-acceptor-labeled RNCs to a three-component model. As noted above, situations in which the donor and acceptor sites are both labeled but no FRET occurs between the two fluorophores cannot be distinguished from nascent chains labeled at the donor site only. Nascent chains with only the Met site fluorescent-labeled did not contribute to the experiment.

A fixed lifetime component (τ_1), with a short lifetime <1.2 ns and a small amplitude $f_1 < 0.10$, is needed to fit the data on all of the samples due to the low fluorophore concentrations (nM). This contribution is presumed to originate from light scattering (Table S2).

We performed curve fitting by using nonlinear least-squares methods, and evaluated the results using the χ^2 value. The fitting routine finds the best possible match between the measured values (phase shift (ϕ_c) and

modulation ratio (M_c)) with the calculated values (phase shift (ϕ_c) and modulation ratio (M_c)) on the basis of the decay law at each frequency. When both phase and modulation data are available, χ^2 is given by

$$\chi^2 = \frac{1}{\nu} \left\{ \sum_{j=1}^N \left[\frac{\phi_e - \phi_c}{\sigma_\phi} \right]^2 + \sum_{j=1}^N \left[\frac{M_e - M_c}{\sigma_M} \right]^2 \right\}, \quad (7)$$

where N is the total number of frequencies; ν is the number of degrees of freedom; and σ_ϕ and σ_M are the phase and modulation standard deviations, which we set constant at values of 0.2 and 0.004, respectively. According to previously reported studies and the instrumental manual, the optimal χ^2 is ~1 and a value < 2 is acceptable (27,28).

The energy transfer efficiency (E_{FRET}) is given by

$$E_{\text{FRET}} = 1 - \left[\frac{(\tau_F^{D+A})}{(\tau_F^D)} \right]. \quad (8)$$

The E_{FRET} is related to the donor-acceptor separation distance (R) by the equation:

$$E_{\text{FRET}} = \frac{1}{[1 + (R/R^0)]^6}, \quad (9)$$

where $R^0 = 57 \text{ \AA}$ for the selected FRET pair here (12).

Recruitment of TF with different RNCs

Various concentrations of TF were included in the cell-free reaction in the TF recruitment experiments. The RNCs were obtained as described earlier and their concentrations were determined by UV absorbance at 260 nm, assuming that 1 unit of A_{260} nm absorption corresponded to 24 nM of 70S ribosomes (29). The TFs that were recruited by the same amount of RNCs were assayed by Western blotting with anti-TF pAb (Genscript, Piscataway, NJ). The blotting signals were analyzed by ImageJ (National Institutes of Health, Bethesda, MD) and ratios of the recruited TF were obtained by normalizing to the system with the highest recruitment, which was obtained with sG at 4 μ M supplemented TF.

RESULTS

Design of nascent chains with poly-A inserts

RNCs comprised of the short nascent polypeptide derived from the N-terminus of GFP (residues 1–34) with two mutations (denoted sG in Fig. 1, A and B) were constructed. To explore the folding state of the nascent chain at different regions within the ribosome tunnel, and to characterize the effects of secondary structure on the recruitment of TF, we replaced a nine-residue fragment in sG by AAAAAAAAA (A₉) either near the exit (2A; Fig. 1 A), at the center of the tunnel (8A; Fig. 1 A), or close to the peptidyl transferase center (17A; Fig. 1 A). This design is based on the finding that A₉ segments may adopt compacted helices within the eukaryotic ribosome tunnel (13,14) and may potentially serve as a helical motif in different zones of the exit tunnel in the RNCs (Fig. 1 A). The detailed sequences are listed in Fig. 1 B.

The compaction of these nascent chains bearing A₉ segments was monitored by TR-FRET studies. The

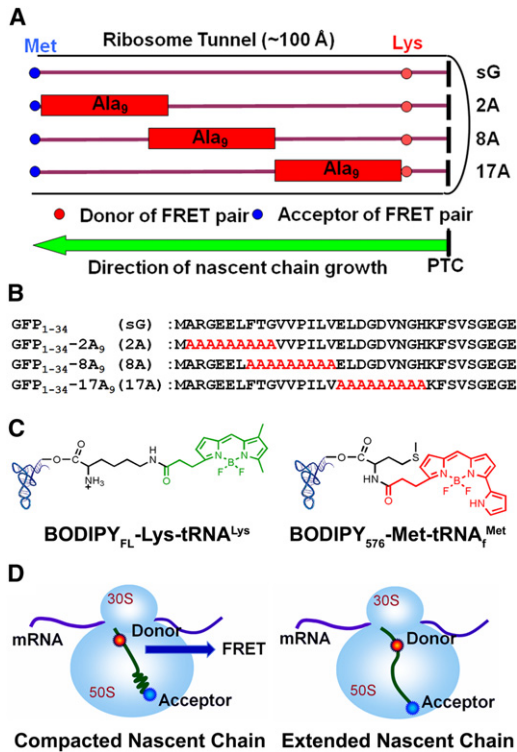


FIGURE 1 Experimental design of the TR-FRET experiments on poly-A-containing RNCs. (A) Schematic of RNCs in the presence and absence of poly-A segments within the ribosome tunnel. The poly-A fragments are shown in rectangles, with the fluorescent donor and acceptor indicated by red and blue circles, respectively. (B) Sequences of sG, 2A, 8A, and 17A. The parent sequences from GFP are in black and the poly-A inserts are in red. (C) Chemical structures of the fluorescent donor (BODIPY_{FL}) and acceptor (BODIPY₅₇₆) attached tRNAs. The fluorophores attached to Lys and Met are colored in green (donor) and red (acceptor), respectively. (D) Schematic of 2A with the poly-A insert in a totally helical (left) or extended (right) conformation. The correlation between E_{FRET} and the donor-acceptor separation distance (R) is described by Eq. 9.

fluorescence donor and acceptor were incorporated into the RNCs (sG, 2A, 8A, and 17A) by covalent attachment of BODIPY_{FL} to Lys²⁶ and BODIPY₅₇₆ to Met¹, respectively, via their corresponding tRNAs (Fig. 1 C). The fluorophores BODIPY_{FL} and BODIPY₅₇₆ were selected as the donor-acceptor pair for their narrow excitation/emission profiles and sufficient spectral overlap for efficient energy transfer ($R^0 = 57 \text{ \AA}$, $n = 1.4$, and $\kappa^2 = 2/3$; Fig. S1) (12). The estimated distance between the donor (Lys²⁶) and acceptor (Met¹) should be $\sim 69.5 \text{ \AA}$ [$9 \times (1.5 \text{ \AA per helical residue}) + 16 \times (3.5 \text{ \AA per extended residue})$] if the poly-A fragment forms an α -helix, and 87.5 \AA [$25 \times (3.5 \text{ \AA per extended residue})$] if the A₉ segment is totally extended. The corresponding E_{FRET} thus ranges from 0.24 to 0.07 for a nascent chain with a compacted A₉ segment to a totally extended nascent chain (Fig. 1 D). Because the length of tunnel is $\sim 100 \text{ \AA}$, all of the nascent chains bearing the poly-A inserts should be embedded within the ribosome tunnel.

Generation of the fluorophore-labeled RNCs

The short, nascent polypeptides with predetermined chain length and attached fluorophores were generated in an *E. coli* in vitro transcription/translation system with anti-oligonucleotide and fluorophore-attached tRNAs (Fig. 2). Labeling of the RNCs was confirmed by Tris-acetate SDS-PAGE and visualized by fluorescence under excitation of 488 nm (donor channel) and 532 nm (acceptor channel; Fig. 2). The acidic SDS-PAGE was used here to preserve the ester bond formed between the tRNA and conjugated polypeptide (24). All nascent chains were shown to be ribosome-bound by application of the puromycin test (Fig. 2). For example, the ribosome-associated nascent polypeptide sG (*p*-tRNA-sG in Fig. 2), linked to the *p*-tRNA at the PTC in the ribosome, was conjugated to puromycin (puromycin-sG in Fig. 2) and released from the ribosome upon puromycin treatment. Some fluorescent tRNA, which could be degraded by RNase A but not released by puromycin, was also observed in the PAGE analysis. It is interesting that the smaller fluorescent tRNA migrates more slowly than the *p*-tRNA-peptide complex during electrophoresis. A possible explanation for this is that the *p*-tRNA-peptide complex has a higher effective charge (more negative) than the tRNA under the acidic buffer system. The anionic denaturant, SDS, can bind to the peptide and contribute sulfate groups to the *p*-tRNA-peptide complex in electrophoresis. On the other hand, the released tRNA may not present itself as a highly negative species in an acidic environment. The isoelectric points of RNA fragments with similar sizes to the tRNA (~ 80 nucleotides) have

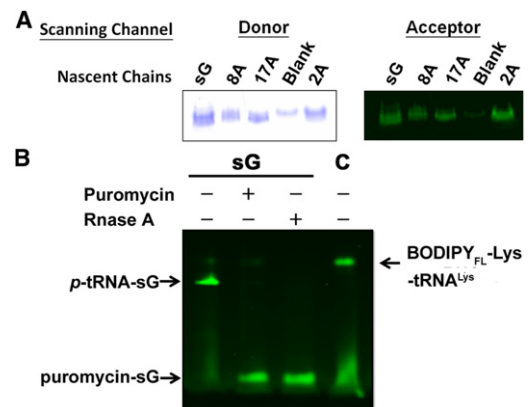


FIGURE 2 PAGE analysis of fluorophore-labeled RNCs. (A) Fluorescence scanning of doubly labeled nascent chains and a blank experiment on SDS-PAGE with scanning of the donor (left panel) and acceptor (right panel) channels (see Materials and Methods). (B) Fluorescence image analysis of the donor-labeled RNCs with puromycin or RNase A treatment. By comparing sG and the free fluorophore-labeled tRNA (denoted C) on the PAGE, one can visualize the fluorescent bands of *p*-tRNA-sG, puromycin-sG, and fluorescent tRNA (BODIPY_{FL}-Lys-tRNA^{Lys}) and identify them by comparing the fluorescent signals before (–) and after (+) the addition of puromycin or RNase A. The smear band observed in the bottom is the hydrolyzed fluorophore during the electrophoresis.

been reported to be higher (between 6.0 and 6.7) (30). Nevertheless, in TR-FRET measurements on a fluorescently labeled tRNA control, we confirmed that the lifetime of the donor attached to the tRNA (~ 5.7 ns, τ_2 , Blank in Table S2) is similar to that on the nascent chains without FRET (~ 5.8 – 6.1 , τ_2 in Table 1), indicating that the background fluorescent tRNA would not interfere with the TR-FRET measurements.

TR-FRET analysis of fluorescent RNCs

The FRET efficiencies for the various fluorescent RNCs were obtained from the fluorescence lifetimes acquired from the time-resolved measurements (Fig. 3 A). The major advantage of TR-FRET is that, compared with steady-state measurements, the donor-acceptor separation distances can be mapped with greater quantitative accuracy. In the time-resolved experiment, the fluorescent lifetimes are insensitive to the local intensity or concentration, and are unaffected by the photobleaching of the fluorophores.

The results derived from the TR-FRET measurements on the four RNCs examined here are summarized in Table 1 and Table S2. As noted earlier, only the dual-labeled RNCs can contribute to a τ_3 component in the analysis of the TR-FRET data. Nascent chains with both donor and acceptor fluorophores exhibit shortened lifetimes if there is FRET between the two fluorophores (τ_3 in Table 1). Whereas the values of τ_2 centered around 5.8–6.1 ns (τ_2 in Table 1) among all nascent chains (plus possible traces of fluorescent tRNA), the τ_3 values were 4.4, 4.2, and 4.1 ns for 2A, 8A, and 17A, respectively. No τ_3 component was required to fit the TR-FRET data for sG. Thus, it is evident that τ_3 corresponds to τ_F^{D+A} , and τ_2 corresponds to τ_F^D , the fluorescence lifetime of donors on nascent chains that are labeled with the donor fluorophore alone, or labeled at both the donor and acceptor sites but without FRET between the two fluorophores. These two scenarios cannot be distinguished from one another, and merge to give an overall τ_2 component in our analysis. The fixed lifetime component (τ_1) was attributed to light scattering, as noted earlier (see also Materials and Methods).

Poly-A-containing nascent chains form a compact conformation in the ribosome tunnel

According to our earlier calculations, if the A_9 insert in the nascent polypeptide adopts a helical conformation within the ribosome tunnel of the RNC, the distance separating the fluorescent donor and acceptor will be ~ 69.5 Å. This distance would give an E_{FRET} of ~ 0.24 in the TR-FRET experiment. Analysis of the E_{FRET} data confirms that the A_9 fragment forms a compacted helix in nascent 2A, 8A, and 17A ($E_{\text{FRET}} \sim 0.3$; Table 1), with FRET distances of 66 ± 5 Å (Fig. 3 B). In contrast, no τ_3 component is needed to fit the TR-FRET data for sG. Thus, the donor and acceptor fluorophores must be too far apart in sG to give an observable FRET, implying an extended conformation in this nascent polypeptide. Therefore, we have successfully generated different RNCs in both extended (sG) and compacted (2A, 8A, and 17A; Fig. 3 C) states. Because the observed compaction is similar in 2A, 8A, and 17A, we surmise that A_9 is forming a helical motif in the different folding zones of the *E. coli* ribosome tunnel. According to their helical propensity (31), these compacted nascent chains do have similar intrinsic tendencies (~ 7 – 9 kcal/mol) to adopt the helix conformation, which is different from sG (~ 13 kcal/mol).

It is possible that the nascent 2A, 8A, and 17A chains in the ribosome tunnel are not structurally homogeneous. In other words, the poly-A segment may not be compacted in all of the nascent polypeptides, but may instead coexist as a mixture of the α -helical fragment and other, more-extended conformations. In the more-extended conformations, the FRET from the donor fluorophore to the acceptor may be too low to contribute to the τ_3 component. On the other hand, if the structure of the A_9 fragments is mostly in the compacted motif, the ratio of f_3/f_2 should reflect the efficiency of incorporating the fluorescently labeled amino acids into the nascent chains. This efficiency of probe incorporation is not available in our experiments, and unfortunately, there is no simple way to directly measure probe incorporation under the conditions used here. However, in a study using the same strategy in a wheat germ cell-free system, it was reported that only 25–30% of the fluorophore-attached amino acids were incorporated into the nascent chains (12). Although there is no basis to assume

TABLE 1 Fluorescence lifetime measurements of fluorescent RNCs

Nascent chain in RNC	Lifetime (ns)*			Fraction of intensity			χ^2	E_{FRET}^\dagger
	τ_1	τ_2 (τ_F^D)	τ_3 (τ_F^{D+A})	f_1	f_2	f_3		
sG	<1.0	5.9 ± 0.1	–	0.03	0.97	–	<1.9	–
2A		5.8 ± 0.1	4.4 ± 0.3	0.05	0.73	0.23	<1.7	0.3 ± 0.1
8A		5.9 ± 0.1	4.2 ± 0.1	0.03	0.85	0.12	<1.1	0.3 ± 0.1
17A		6.0 ± 0.1	4.1 ± 0.7	0.02	0.67	0.31	<1.2	0.3 ± 0.1

*Represented lifetimes are means \pm SD. The total number of measurements from independent experiments, n , is 3–6.

† Energy transfer efficiency, E_{FRET} , is calculated from Eq. 8. According to the p -value in the t -test, the τ_F^{D+A} values measured for the poly-A samples were significantly different from the corresponding τ_F^D values ($p \sim 0.001$).

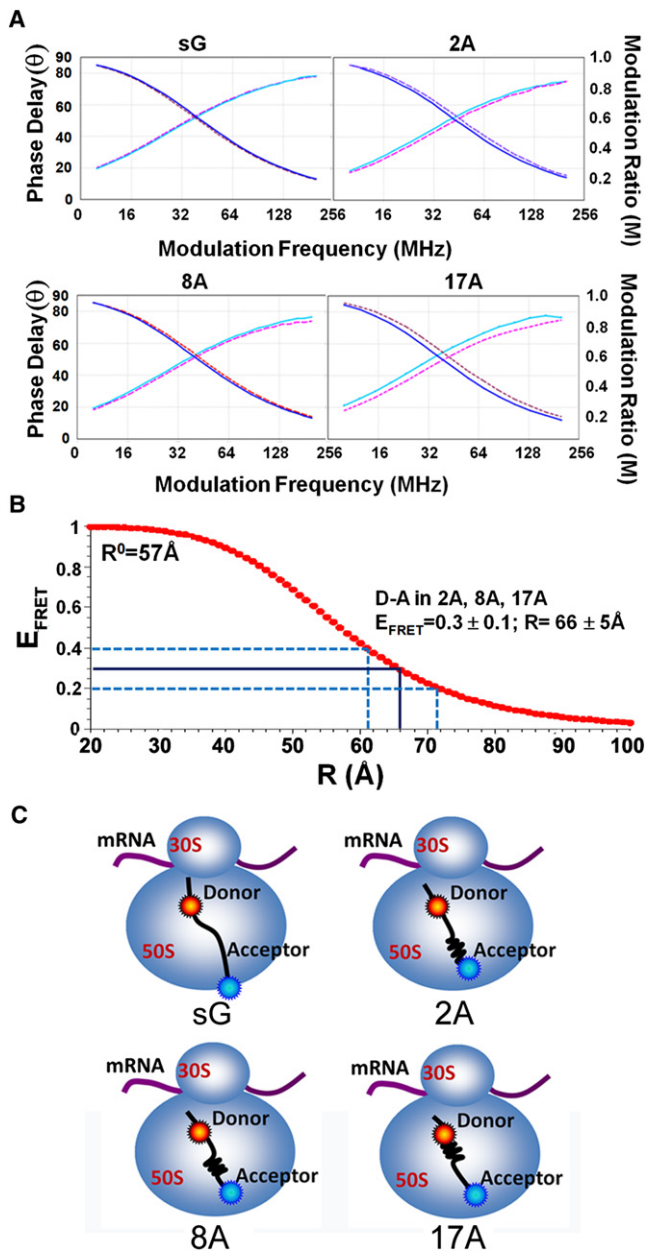


FIGURE 3 Poly-A-containing nascent chains form a compacted conformation in the tunnel. (A) The lifetime measurements of the RNCs (sG, 2A, 8A, and 17A) were determined with the use of a frequency-domain fluorimeter. Data are shown for the donor-labeled samples (solid line) and double-labeled samples (dashed line). (B) The distance between the fluorophore pairs in different RNCs, derived from Eq. 9 and the measured E_{FRET} (Table 1) with $R^0 = 57 \text{\AA}$. (C) Representations of the structures of the nascent chains associated with the different RNCs. The poly-A fragments are shown as compacted helices in 2A, 8A, and 17A.

that the bacterial and wheat germ systems should behave similarly in this regard, it turns out the f_3/f_2 ratios are not so sensitive to the efficiency of probe incorporation provided that a sufficient number of the nascent chains are dual-labeled with the fluorescent-labeled amino acids, and the structure of the A_9 fragments is in the compacted motif

in a substantial fraction of these nascent polypeptides. As an illustration, the ratio of dual-labeled nascent chains to donor-labeled nascent chains (0.2) is similar to the ratio of f_3/f_2 that we observed for 8A in our TR-FRET experiments, if one assumes a similar efficiency (25–30%) for incorporating the fluorescent donor and acceptor into our *E. coli* cell-free system as in the wheat germ system. (The measured f_3/f_2 ratios are 0.15, 0.3, and 0.45 for 8A, 2A, and 17A, respectively.) According to our analysis (Table S3), a higher observed f_3/f_2 ratio can only come about with a higher efficiency of incorporation of the fluorescent-labeled amino acids into the nascent polypeptides, and then only with the A_9 fragments in these nascent chains being mostly compacted (>75%) within the ribosome tunnel. Thus, although our experimental design does not permit measurements of the extent of probe incorporation, a shortcoming that does place certain limits on the interpretation of our results, the caveat that some of the A_9 fragments in the nascent 2A, 8A, and 17A chains may not be compacted in the ribosome tunnel should not detract from the general conclusion that we have derived from this study (vide infra) relating to the effect of the compaction on ribosome function.

To demonstrate that the FRET observed for the nascent polypeptides with the A_9 inserts results mainly from the compaction of the poly-A segment, we added back six amino acids of the parent sequences to 2A, 8A, and 17A right behind the nine inserted alanines, and remeasured the FRET efficiency in the extended nascent polypeptides $2A^+$, $8A^+$, and $17A^+$ (Fig. 4 B). If the additional amino acids introduced could be induced to form helices, the extended nascent chain should still give significant FRET signals (calculated distance: 78.5 \AA ; calculated FRET efficiency: 0.13). As expected, no FRET was observed in $2A^+$, $8A^+$, or $17A^+$, indicating that the parent sequences added to form these extended nascent polypeptides were mostly in an extended state (calculated distance: 90.5 \AA ; calculated FRET efficiency: 0.06). Of more importance, these experiments allowed us to move each of the A_9 structural motifs some 21 \AA farther toward the tunnel exit, and, in fact, in the case of nascent polypeptide $2A^+$, the poly-A insert should be outside of the ribosome tunnel. Details of the TR-FRET measurements on $2A^+$, $8A^+$, and $17A^+$ are shown in Table S4 and Fig. S3.

The high FRET efficiency between the same donor/acceptor pair observed by Woolhead et al. (12) on nascent chains of membrane proteins, together with the results presented here, suggests that most of the ribosome exit tunnel is capable of accommodating the helical conformation of nascent chains in the wheat germ and the *E. coli* ribosome. On the other hand, on the basis of a biochemical analysis of poly-A nascent chain compaction by Lu and Deutsch (13), as well as cryo-EM studies by Bhushan et al. (14), it was proposed that the helix is mainly formed at the beginning or the bottom of the tunnel, but not in the middle region,

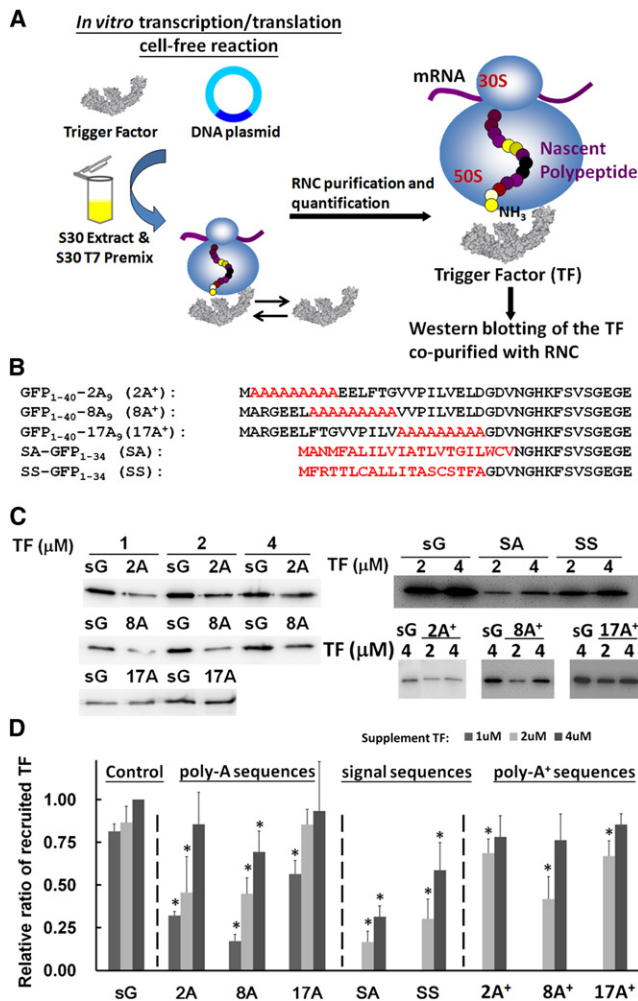


FIGURE 4 Poly-A and signal peptide containing RNCs decrease the recruitment of TF. (A) A schematic of the generation and characterization of the TF-RNCs. (B) Amino acid sequence alignment of the extended poly-A peptide (2A⁺, 8A⁺, and 17A⁺) and the signal peptide (SA and SS) on the RNCs. The parent amino acid sequences from GFP are in black and the inserted/substituted amino acids are in red. (C) Western blotting of the TF recruited by different RNCs (sG, 2A, 8A, 17A, 2A⁺, 8A⁺, 17A⁺, SA, and SS) with varying amounts of external TF (for details see [Materials and Methods](#)). (D) Ratios of the recruited TF relative to that recruited by sG with a 4 μM TF supplement. All experiments were repeated three to nine times, and the data are represented by means ± SD. Nascent chains that showed a significant difference (*p* smaller than 0.01) in TF recruitment from the sG control according to the *t*-test are highlighted by an asterisk (TF recruitments were performed with the same amount of TF supplement).

in the case of the wheat germ and the rabbit ribosome. At present, we are not sure whether these different observations are due to the different biological species or different analytical tools (FRET versus chemical modification and cryo-EM) used to monitor the compaction. Although the descriptions of the folding zones differ slightly among these studies, they all suggest that the nascent chains bearing poly-A, alanine-rich, or membrane sequence can adopt the α -helical conformation in the ribosome tunnel.

RNCs bearing either a compacted poly-A or signal sequence appear to lessen the recruitment of TF in a zone-specific manner

Interestingly, the folding state of the nascent polypeptide within the tunnel may influence chaperone recruitment. We examined the ability of seven RNCs to bind to TF, the ribosome-associated chaperone that provides a protective crevice from protease cleavage and serves as a folding cradle for the nascent proteins emerging from ribosome (17). Various concentrations (1–4 μM) of recombinant TF were added to the cell-free system and the ribosome-bound TF complexes were copurified with the RNCs, followed by Western blotting with TF antibody (Fig. 4 A). The TF recruitment by the RNCs containing 2A, 8A, and 17A were compared with the corresponding recruitment by sG at various concentrations of supplemented TF (Fig. 4 C). We found that the TF recruitment was significantly reduced in 2A and 8A, but only slightly reduced in 17A. At 1 μM TF, the recruited TF ratio (recruited TF/recruited TF by sG) followed the trend: sG (0.8) > 17A (0.6) > 2A (0.3) > 8A (0.2) (Fig. 4 D). In the case of sG and 17A, the TF recruitment was found to be insensitive to the initial TF concentration. However, higher amounts of TF were required in the case of 2A and 8A, indicating weaker TF binding. The degree of TF binding thus seems to depend on the location of the helical motif within the exit tunnel in the RNCs. Moreover, the recruitment of TF was somewhat affected in the case of 8A⁺ but not in 2A⁺ or 17A⁺, when compared with sG (Fig. 4, C and D). These results regarding TF recruitment are detailed in [Table S5](#).

For comparison, two RNCs containing signal sequences (SA-RNC and SS-RNC) were also generated. The SA-RNC harbors a signal anchor (SA) sequence from a cytoplasmic membrane protein (leader peptidase MANMFA LILVIATLVTGILWCV), and SS-RNC includes a signal sequence (SS) from a secretory protein (pre- β -lactamase, MFRTTLCALLITASCSTFA; Fig. 4 B) (32). Presumably, these signal sequences form helices within the ribosome tunnel (12,33). Moreover, the SA and SS signal sequences have been reported to enhance the recruitment of SRP to the RNCs while they are still residing in the ribosome tunnel (32,34).

Compared with poly-A-containing RNCs, we found that the SA- and SS-RNCs recruited significantly less TF than sG (Fig. 4, C and D). In fact, the SA-RNC has the lowest binding affinity for TF among all the RNCs (recruited TF ratio relative to sG: ~0.2 and 0.3 at TF concentrations of 2 μM and 4 μM, respectively). From a cryo-EM reconstruction of SRP-RNCs structure and FRET studies, it was previously surmised that the signal sequences form compacted structural motifs within the tunnel (12,33). In this study, the nascent chains SA and SS span the same region of the tunnel that is presumably occupied by the poly-A motif in 2A and 8A. Therefore, the data are consistent with the

hypothesis that the compacted conformation of the nascent chains within the tunnel may influence the recruitment of TF in a zone-specific manner.

We also considered whether the hydrophobicity of these nascent chains contributes to the TF recruitment. The hydrophobicity of sG, 2A, 8A, 17A, SS, and SA was obtained by total or local hydrophobicity analysis (35,36). The results showed that there is no correspondence of the TF recruitment with the predicted trend in the hydrophobicity of these nascent chains (Fig. S5). The total hydrophobicity (kcal/mol) of these nascent chains followed the trend (from the highest to the lowest) SA (4.5) > SS (16) > 17A (20.5) > 2A (26) > sG (30.6) > 8A (39.1). The local hydrophobicity analysis revealed that many amino acids with high mean hydrophobicity (-0.5 kcal/mol) were found in SA ($n = 14$), 17A ($n = 10$), and 2A ($n = 8$), but only a few were found in sG ($n = 3$), and they were absent in 8A and SS (Fig. S5).

DISCUSSION

Possible regions in the ribosome that interact with RNCs and interfere with TF recruitment

Earlier work allowed us to map the regions of the exit tunnel where a helical motif might interfere with the TF recruitment. From x-ray and cryo-EM reconstituted structures of the ribosome, the exit tunnel appears to be created by the three tunnel-associated ribosomal proteins, L4, L22, and L23 (Fig. 5 A) (5,6). We aligned all of the nascent chains examined in this study and compared them within the ribosome tunnel (Fig. 5 A). Except in the case of 17A, 2A⁺, and 17A⁺, we find that the poly-A segments in the remaining nascent chains, namely, 2A, 8A, and 8A⁺, as well as a portion of the SA and SS sequences, may be in contact with L23.

When we compare the TF recruitment between 2A and 2A⁺, we find that 2A⁺ has lost the ability to reduce the TF recruitment, which is expected because the poly-A segment in 2A⁺ is now outside of the ribosome tunnel and can no longer interact with L23 (Fig. 5 A). Between 8A and 8A⁺, a noticeable reduction in TF recruitment is still observed. Here, when we align the nascent chain sequence of 8A⁺ against that of sG, it appears that the A₉ segment in 8A⁺ might still be able to interact with L23. Accordingly, we surmise that the reduction in the recruitment of TF might be brought about by the introduction of the A₉ helical motif to the region associated with L23. We conclude that the change in TF binding is not related to the loss of specific residues in the parent sG sequence, but is instead associated with the presence and location of the poly-A compaction at the bottom 35 Å portion of the tunnel (in 2A, 8A, 8A⁺, SA, and SS). Although the whole tunnel might permit helix formation, it is the bottom portion that modulates TF recruitment.

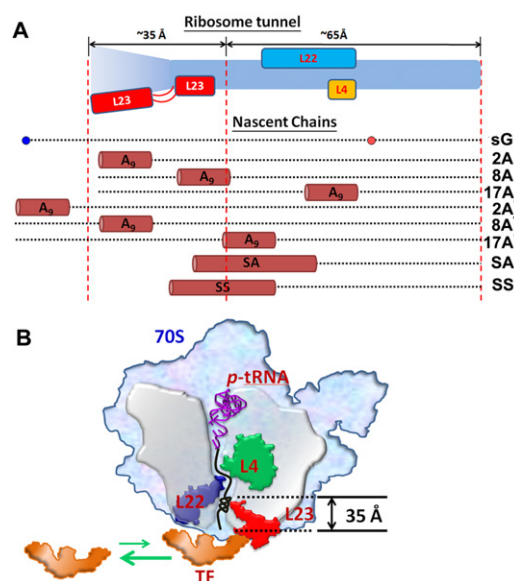


FIGURE 5 Possible interacting zones between the ribosome tunnel and the nascent chains suggested by the ribosome crystal structure (5,6) and our experimental results. (A) Possible locations of our nascent chains in the tunnel. The ribosome tunnel is colored in light blue, and the three ribosomal proteins that may interact directly with nascent chains in the tunnel are in yellow (L4), blue (L22), and red (L23) block, respectively. For easier comparison, the compact poly-A and signal sequence fragments on the nascent chains are shown as tubes and the parent GFP fragments are shown as dotted lines. The region of the ribosome tunnel 35 Å from the tunnel exit that includes the L23 is proposed to be important for TF recruitment. (B) A model of the compacted nascent chains (e.g., 8A) within the bottom of the tunnel that may interact with L23 and influence TF recruitment.

It is significant that compaction of the nascent polypeptide chain within the ribosome exit tunnel can influence TF recruitment. In this study, the A₉ helical motif was judiciously placed in different regions of the ribosome exit tunnel to facilitate the transmission of different allosteric signals to the TF-binding surface outside the ribosome tunnel when the compacted helix is interacting with the inside walls of the tunnel in the different zones. The experimental results we obtained for the SA- and SS-RNCs are in good agreement with these conclusions, because these signal peptides presumably form a compacted structural motif that may interact with L23 as in 2A, 8A, and 8A⁺.

Possible competition between TF and SRP binding on L23

Only one ribosomal protein, L23, is associated with the bottom 35 Å portion of the tunnel, and TF binds to the external surface of L23 in the ribosome structure (5). We conjecture that there is an interaction between the helical motif in the different RNCs (2A, 8A, 8A⁺, SA, and SS) and the loop of L23 lining the tunnel that triggers a conformational signal to the TF-binding surface of L23 to regulate the recruitment of TF.

It is known that L23 provides the general docking site for both TF and SRP (1). Several biochemical and biophysical studies indicate that SRP has a strong association with L23 when a signal sequence is present in the exit tunnel of the ribosome (16,32,34). In this study, we have shown that TF recruitment is substantially diminished when signal sequences occupy the L23-associated region within the tunnel (Fig. 5 B). Although the notion is still under debate, the binding of TF and SRP may be mutually exclusive, in that a helical motif in this region of the exit tunnel decreases the binding affinity of TF and presumably enhances the affinity of the ribosome for SRP. In fact, a reduction of TF binding to the RNC is essential to ensure that the SRP takes over from the TF in the cotranslational folding of membrane/secretory proteins to increase the accuracy of recognition of the nascent chain during protein targeting. In this manner, depending on whether a polypeptide is targeted for the membrane/secretion or the cytosol, the nascent chain can become associated with the SRP, or fold spontaneously with the assistance of the TF chaperone, when it emerges from the exit tunnel (18–20,37). Interestingly, a recent study showed that SecA, which has been proposed to recognize secretory proteins post-translationally, is also capable of interacting with L23 (38). This striking result adds further complexity to the issue of competitive binding of chaperones on the ribosome surface.

CONCLUSION

In this work we have provided different examples to demonstrate that cotranslational protein folding within the ribosome tunnel may affect chaperone recruitment. By relocating the position of the poly-A segment within the tunnel, we found that we could modulate TF recruitment. Although the mechanistic details remain to be explored, it is clear that L23 plays an important role in the protein translocation process (32).

SUPPORTING MATERIAL

Five tables and five figures are available at [http://www.biophysj.org/biophysj/supplemental/S0006-3495\(S0006-3495\(12\)00523-1](http://www.biophysj.org/biophysj/supplemental/S0006-3495(S0006-3495(12)00523-1).

We thank Prof. Wei-Hau Chang, Dr. Li-Ling Yang, Dr. Hsin-Liang Chen, and members of the Huang laboratory for comments on the manuscript.

This work was supported by research grants from the National Science Council, Taiwan (NSC 97-2113-M-001-003-MY2 and NSC 98-2113-M-001-015-MY2). K.-F.L. was supported by a postdoctoral fellowship from Academia Sinica.

REFERENCES

- Kramer, G., D. Boehringer, ..., B. Bukau. 2009. The ribosome as a platform for co-translational processing, folding and targeting of newly synthesized proteins. *Nat. Struct. Mol. Biol.* 16:589–597.
- Ban, N., P. Nissen, ..., T. A. Steitz. 2000. The complete atomic structure of the large ribosomal subunit at 2.4 Å resolution. *Science*. 289:905–920.
- Voss, N. R., M. Gerstein, ..., P. B. Moore. 2006. The geometry of the ribosomal polypeptide exit tunnel. *J. Mol. Biol.* 360:893–906.
- Beckmann, R., C. M. Spahn, ..., G. Blobel. 2001. Architecture of the protein-conducting channel associated with the translating 80S ribosome. *Cell*. 107:361–372.
- Ferbitz, L., T. Maier, ..., N. Ban. 2004. Trigger factor in complex with the ribosome forms a molecular cradle for nascent proteins. *Nature*. 431:590–596.
- Seidelt, B., C. A. Innis, ..., R. Beckmann. 2009. Structural insight into nascent polypeptide chain-mediated translational stalling. *Science*. 326:1412–1415.
- Woolhead, C. A., A. E. Johnson, and H. D. Bernstein. 2006. Translation arrest requires two-way communication between a nascent polypeptide and the ribosome. *Mol. Cell*. 22:587–598.
- Nakatogawa, H., and K. Ito. 2002. The ribosomal exit tunnel functions as a discriminating gate. *Cell*. 108:629–636.
- Yap, M. N., and H. D. Bernstein. 2009. The plasticity of a translation arrest motif yields insights into nascent polypeptide recognition inside the ribosome tunnel. *Mol. Cell*. 34:201–211.
- Mitra, K., C. Schaffitzel, ..., J. Frank. 2006. Elongation arrest by SecM via a cascade of ribosomal RNA rearrangements. *Mol. Cell*. 22:533–543.
- Dresios, J., I. L. Derkatch, ..., D. Synetos. 2000. Yeast ribosomal protein L24 affects the kinetics of protein synthesis and ribosomal protein L39 improves translational accuracy, while mutants lacking both remain viable. *Biochemistry*. 39:7236–7244.
- Woolhead, C. A., P. J. McCormick, and A. E. Johnson. 2004. Nascent membrane and secretory proteins differ in FRET-detected folding far inside the ribosome and in their exposure to ribosomal proteins. *Cell*. 116:725–736.
- Lu, J., and C. Deutsch. 2005. Folding zones inside the ribosomal exit tunnel. *Nat. Struct. Mol. Biol.* 12:1123–1129.
- Bhushan, S., M. Gartmann, ..., R. Beckmann. 2010. α -Helical nascent polypeptide chains visualized within distinct regions of the ribosomal exit tunnel. *Nat. Struct. Mol. Biol.* 17:313–317.
- Kosolapov, A., and C. Deutsch. 2009. Tertiary interactions within the ribosomal exit tunnel. *Nat. Struct. Mol. Biol.* 16:405–411.
- Peterson, J. H., C. A. Woolhead, and H. D. Bernstein. 2010. The conformation of a nascent polypeptide inside the ribosome tunnel affects protein targeting and protein folding. *Mol. Microbiol.* 78:203–217.
- Hoffmann, A., B. Bukau, and G. Kramer. 2010. Structure and function of the molecular chaperone Trigger Factor. *Biochim. Biophys. Acta*. 1803:650–661.
- Raine, A., M. Lovmar, ..., M. Ehrenberg. 2006. Trigger factor binding to ribosomes with nascent peptide chains of varying lengths and sequences. *J. Biol. Chem.* 281:28033–28038.
- Kaiser, C. M., H. C. Chang, ..., J. M. Barral. 2006. Real-time observation of trigger factor function on translating ribosomes. *Nature*. 444:455–460.
- Rutkowska, A., M. P. Mayer, ..., B. Bukau. 2008. Dynamics of trigger factor interaction with translating ribosomes. *J. Biol. Chem.* 283:4124–4132.
- Lee, J., M. K. Shin, ..., W. S. Ryu. 2010. Insertion and deletion mutagenesis by overlap extension PCR. *Methods Mol. Biol.* 634:137–146.
- Lin, K. F., T. R. Lee, ..., P. C. Lyu. 2007. Structure-based protein engineering for α -amylase inhibitory activity of plant defensin. *Proteins*. 68:530–540.
- Gite, S., S. Mamaev, ..., K. Rothschild. 2000. Ultrasensitive fluorescence-based detection of nascent proteins in gels. *Anal. Biochem.* 279:218–225.

24. Kirchdoerfer, R. N., J. J. Huang, ..., S. Cavagnero. 2007. Fluorescence-based analysis of aminoacyl- and peptidyl-tRNA by low-pH sodium dodecyl sulfate-polyacrylamide gel electrophoresis. *Anal. Biochem.* 364:92–94.
25. Ellis, J. P., C. K. Bakke, ..., S. Cavagnero. 2008. Chain dynamics of nascent polypeptides emerging from the ribosome. *ACS Chem. Biol.* 3:555–566.
26. Hanes, J., and A. Plückthun. 1997. In vitro selection and evolution of functional proteins by using ribosome display. *Proc. Natl. Acad. Sci. USA.* 94:4937–4942.
27. DeLong, L. J., and J. W. Nichols. 1996. Time-resolved fluorescence anisotropy of fluorescent-labeled lysophospholipid and taurodeoxycholate aggregates. *Biophys. J.* 70:1466–1471.
28. Szmajcinski, H., W. Wiczak, ..., M. L. Johnson. 1996. Distance distributions from the tyrosyl to disulfide residues in the oxytocin and [Arg8]-vasopressin measured using frequency-domain fluorescence resonance energy transfer. *Eur. Biophys. J.* 24:185–193.
29. Kurland, C. G. 1966. The requirements for specific sRNA binding by ribosomes. *J. Mol. Biol.* 18:90–108.
30. Sherbet, G. V., M. S. Lakshmi, and F. Cajone. 1983. Isoelectric characteristics and the secondary structure of some nucleic acids. *Biophys. Struct. Mech.* 10:121–128.
31. Pace, C. N., and J. M. Scholtz. 1998. A helix propensity scale based on experimental studies of peptides and proteins. *Biophys. J.* 75:422–427.
32. Bornemann, T., J. Jöckel, ..., W. Wintermeyer. 2008. Signal sequence-independent membrane targeting of ribosomes containing short nascent peptides within the exit tunnel. *Nat. Struct. Mol. Biol.* 15:494–499.
33. Halic, M., M. Blau, ..., R. Beckmann. 2006. Following the signal sequence from ribosomal tunnel exit to signal recognition particle. *Nature.* 444:507–511.
34. Berndt, U., S. Oellerer, ..., S. Rospert. 2009. A signal-anchor sequence stimulates signal recognition particle binding to ribosomes from inside the exit tunnel. *Proc. Natl. Acad. Sci. USA.* 106:1398–1403.
35. Wimley, W. C., and S. H. White. 1996. Experimentally determined hydrophobicity scale for proteins at membrane interfaces. *Nat. Struct. Mol. Biol.* 3:842–848.
36. Roseman, M. A. 1988. Hydrophilicity of polar amino acid side-chains is markedly reduced by flanking peptide bonds. *J. Mol. Biol.* 200:513–522.
37. Ullers, R. S., E. N. Houben, ..., J. Lührink. 2006. Sequence-specific interactions of nascent *Escherichia coli* polypeptides with trigger factor and signal recognition particle. *J. Biol. Chem.* 281:13999–14005.
38. Huber, D., N. Rajagopalan, ..., B. Bukau. 2011. SecA interacts with ribosomes in order to facilitate posttranslational translocation in bacteria. *Mol. Cell.* 41:343–353.